vibrations, as established by other experiments (figs. S4 to S6) (*14*).

The spatial organization of the frequency response along the dorsal cuticle is in stark contrast with that of the TM and TP. Low frequencies dominate at the proximal end (P1 in Fig. 4A), whereas high frequencies prevail distally (P7 in Fig. 4A; see also fig. S5). This is a hallmark of tonotopy. This organization conforms to the tonotopic sensitivities of CA mechanoreceptors (Fig. 2D) (*11*). Intermediate locations (P2 to P6) exhibit a gradual increase in frequency response.

The definitive characteristics of mammalian cochlear-frequency analyzers are the essential unidirectional traveling waves, discovered by Georg von Békésy (*3*). These features are paralleled at the microscale in katydids by the mechanical deflections observed along the dorsal cuticle (Fig. 4A, yellow line). Traveling waves are initiated distally and travel toward proximal locations of the AV, as recorded through the dorsal cuticle (Fig. 4B and movie S3). A 23-kHz four-cycle tone elicits four oscillations that all reach an identical physical destination, located 200 μm along the transect around location P3-P4 (Fig. 4, A and B). The first cycle elicits a sinusoidal response first located at ~100 μm (Fig. 4B, black arrow), which then moves toward the 200-μm mark (Fig. 4B, white arrow) within 22 μs (half-period at 23 kHz). The oscillation reaches its maximum displacement velocity (red and blue peaks in Fig. 4B) at this position (200 μm), before rapidly decaying over a further 25 μm. The next three cycles generate the same oscillations with increased magnitude at this location. The presence of a wave traveling from distal to proximal locations along the CA corroborates results from another katydid species (*13*). Other frequencies (5 to 50 kHz) also elicit this pattern but reach maximal magnitude at different locations (Fig. 4D). The dispersive nature of AV waves is best illustrated by the presence of phase accumulation, as waves travel across the dorsal cuticle. High-frequency waves (40 to 50 kHz) incur some 260° phase lag within a 200-μm travel length, whereas low-frequency waves (10 kHz), traveling 400 μm, accumulate up to 300° (Fig. 4C). The velocity of wave propagation varies with frequency from 4 ms^{-1} (10 kHz) to 8 ms^{-1} (50 kHz), exhibiting a pattern similar to those reported for mammals and other insects (*13*, *19*).

Deflection shape analysis conducted in the spectral domain (5- to 50-kHz sweeps) confirms the unambiguous presence of traveling waves (fig. S6) (*14*). The data imply that AV provides the anisotropic medium enabling dispersive wave propagation and tonotopic delivery to the auditory receptors. Further experiments establish that both an intact AV and its fluid are required for frequency decomposition as well as for generation of traveling waves (fig. S7). In contrast to observations from the phaneropterine katydid *Mecopoda elongata* (*13*), removal of the dorsal cuticle in *C. gorgonensis* markedly alters AV integrity and eliminates traveling waves and dispersive propagation (*14*).

Altogether, the data show that the impedance conversion, dispersive wave propagation, and tonotopic representation are biophysically analogous to the same qualities of the mammalian cochlea. For *C. gorgonensis*, however, the entire process is embedded in morphology about one to two orders of magnitude smaller than that of mammals (centimeters and millimeters to micrometers).

Frequency representation along the AV covers 10 to 50 kHz (Fig. 4D), a range much larger than that of the natural song (FM: 23.5 to 18.2 kHz) (Fig. 2A) (*6*). Notably, only a short AV segment of ~40 μm represents the song's FM (n = 21 animals) (Fig. 4D). For other frequencies, tonotopic mapping is spatially more disperse (Fig. 4D and fig. S6), suggesting that *C. gorgonensis* can hear other sounds in addition to its own song, such as the ultrasonic sounds of predators (e.g., echolocating bats) (*20*).

As in mammals, impedance matching in katydids arises from the surface area ratio between the TM and TP and from the lever resulting from their coupled action (Fig. 1). Both cases are evolutionarily convergent; the result is the efficient transfer of vibrations to the fluid- or lipid-filled channel (the cochlea or the AV, respectively) where mechanosensory cells reside. Sophisticated hearing is possible at the microscale; katydid ears provide valuable inspiration for the construction of miniaturized smart acoustic sensors, contributing to the expanding panoply of insect-inspired technology.

References and Notes

1. W. Bialek, *Annu. Rev. Biophys. Biophys. Chem.* **16**, 455 (1987).
2. A. J. Hudspeth, *Nature* **341**, 397 (1989).
3. G. von Békésy, *Experiments in Hearing* (McGraw-Hill, New York, 1960).
4. J. Ashmore, *Physiol. Rev.* **88**, 173 (2008).
5. L. Robles, M. A. Ruggero, *Physiol. Rev.* **81**, 1305 (2001).
6. F. Montealegre-Z, M. Postles, *J. Orthoptera Res.* **19**, 347 (2010).
7. J. E. Yack, *Microsc. Res. Tech.* **63**, 315 (2004).
8. M. Bangert *et al.*, *Hear. Res.* **115**, 27 (1998).
9. D. B. Lewis, *J. Exp. Biol.* **60**, 839 (1974).
10. K. Kalmring, W. Rossler, R. Ebendt, J. Ahi, R. Lakes, *Zool. Jahrb. Allg. Zool.* **97**, 75 (1993).
11. B. P. Oldfield, *J. Comp. Physiol.* **147**, 461 (1982).
12. R. R. Hoy, D. Robert, *Annu. Rev. Entomol.* **41**, 433 (1996).
13. A. Palghat Udayashankar, M. Kössl, M. Nowotny, *PLoS ONE* **7**, e31008 (2012).
14. Materials and methods are available as supplementary materials on *Science* Online.
15. M. Nowotny, J. Hummel, M. Weber, D. Möckel, M. Kössl, *J. Comp. Physiol. A Neuroethol. Sens. Neural Behav. Physiol.* **196**, 939 (2010).
16. R. Boistel *et al.*, *PLoS ONE* **6**, e22080 (2011).
17. J. Mueller, L. A. Tsuji, *PLoS ONE* **2**, e889 (2007).
18. H. A. Thomassen *et al.*, *Hear. Res.* **225**, 25 (2007).
19. J. F. C. Windmill, M. C. Göpfert, D. Robert, *J. Exp. Biol.* **208**, 157 (2005).
20. J. J. Belwood, G. K. Morris, *Science* **238**, 64 (1987).

Acknowledgments: This work was sponsored by the Human Frontier Science Program (Cross Disciplinary Fellowship LT00024/2008-C to F.M.-Z.). D.R. is supported by the Royal Society of London. This research was also partially supported by the UK–India Education and Research Initiative (grant no. SA06-169E) and the Biotechnology and Biological Sciences Research Council. We declare no conflict of interest. The Colombian Ministry of Environment granted a permit for fieldwork at Gorgona National Park (decree DTSO-G-31 11/07). All additional information regarding data generation is given in the text and the supplementary materials.

Supplementary Materials

www.sciencemag.org/cgi/content/full/338/6109/968/DC1
Materials and Methods
Supplementary Text
Figs. S1 to S7
Table S1
References (*21*–*32*)
Movies S1 to S3

28 May 2012; accepted 25 September 2012
10.1126/science.1225271

Offspring from Oocytes Derived from in Vitro Primordial Germ Cell–like Cells in Mice

Katsuhiko Hayashi,[1,2,3]* Sugako Ogushi,[1,4] Kazuki Kurimoto,[1,5] So Shimamoto,[1] Hiroshi Ohta,[1,5] Mitinori Saitou[1,2,5,6]*

Reconstitution of female germ cell development in vitro is a key challenge in reproductive biology and medicine. We show here that female (XX) embryonic stem cells and induced pluripotent stem cells in mice are induced into primordial germ cell–like cells (PGCLCs), which, when aggregated with female gonadal somatic cells as reconstituted ovaries, undergo X-reactivation, imprint erasure, and cyst formation, and exhibit meiotic potential. Upon transplantation under mouse ovarian bursa, PGCLCs in the reconstituted ovaries mature into germinal vesicle-stage oocytes, which then contribute to fertile offspring after in vitro maturation and fertilization. Our culture system serves as a robust foundation for the investigation of key properties of female germ cells, including the acquisition of totipotency, and for the reconstitution of whole female germ cell development in vitro.

The germ cell lineage in mammals originates from pluripotent epiblasts as primordial germ cells (PGCs) and undergoes sexually dimorphic development, generating spermatozoa in males and oocytes in females. These cells fertilize to form zygotes with full developmental

potential, serving as the foundation of the mammalian life cycle. We have shown previously that embryonic stem cells (ESCs) and induced pluripotent stem cells (iPSCs) from male (XY) mice are induced into epiblast-like cells (EpiLCs), which, in turn, are induced into primordial germ cell–like cells (PGCLCs) with proper function for spermatogenesis and offspring production (*1*). Considering the differences between male (XY) and female (XX) ESCs, including those at the epigenetic level (*2*), together with the markedly different mechanisms of male and female germ cell development (*3*), a fundamental challenge remains to determine whether our system reconstitutes the female developmental pathway and whether PGCLCs serve as precursors for fully functional oocytes.

To explore this possibility, we derived female ESCs bearing *Prdm1* (also known as *Blimp1*)–*mVenus* and *Dppa3* (also known as *stella*)–*ECFP* (BVSC) transgenes (*Prdm1* and *Dppa3* show specific expression in PGCs) (*4*) and induced them into EpiLCs and further into PGCLCs (see supplementary materials and methods). The dynamics of EpiLC and PGCLC induction from the female ESCs (the H18 and H14 lines) appeared similar to those from male ESCs (fig. S1) (*1*). To further characterize female PGCLCs, we chose the strategy of "reconstituted ovaries": One can aggregate female PGCs with embryonic gonadal somatic cells to form reconstituted ovaries in vitro, which are then transplanted under ovarian bursa or kidney capsules of recipient mice for oogenesis (Fig. 1A) (*5*, *6*). The H18 ESCs were induced into PGCLCs, and, at each time point from day 3 (d3) to day 6 (d6) of PGCLC induction, the BV-positive cells were sorted by fluorescence-activated cell sorting and reaggregated with E12.5 (embryonic day 12.5) gonadal somatic cells (1000 PGCLCs plus 10,000 somatic cells) for further culture (Fig. 1A and fig. S2A). The d3 PGCLCs exhibit robust proliferation in reconstituted ovaries (fig. S2 and supplementary text) and, with regard to gene expression and epigenetic profiles (X inactivation or reactivation and imprinting), undergo a developmental progression similar to that of PGCs in embryonic ovaries, reaching, at day 6 in reconstituted ovaries (d3ag6), a premeiotic stage similar to E12.5 PGCs (Fig. 1, B

[1]Department of Anatomy and Cell Biology, Graduate School of Medicine, Kyoto University, Yoshida-Konoe-cho, Sakyo-ku, Kyoto 606-8501, Japan. [2]Center for iPS Cell Research and Application, Kyoto University, 53 Kawahara-cho, Shogoin Yoshida, Sakyo-ku, Kyoto 606-8507, Japan. [3]Japan Science and Technology Agency (JST), Core Research for Evolutional Science and Technology, Japan Science and Technology Agency (CREST)/Precursory Research for Embryonic Science and Technology (PRESTO), Yoshida-Konoe-cho, Sakyo-ku, Kyoto 606-8501, Japan. [4]The Hakubi Center for Advanced Research, Kyoto University, Yoshida-Ushinomiya-cho, Sakyo-ku, Kyoto 606-8302, Japan. [5]JST, CREST/Exploratory Research for Advanced Technology (ERATO), Yoshida-Konoe-cho, Sakyo-ku, Kyoto 606-8501, Japan. [6]Institute for Integrated Cell-Material Sciences, Kyoto University, Yoshida-Ushinomiya-cho, Sakyo-ku, Kyoto 606-8501, Japan.

*To whom correspondence should be addressed. E-mail: saitou@anat2.med.kyoto-u.ac.jp (M.S.); khayashi@anat2.med.kyoto-u.ac.jp (K.H.)

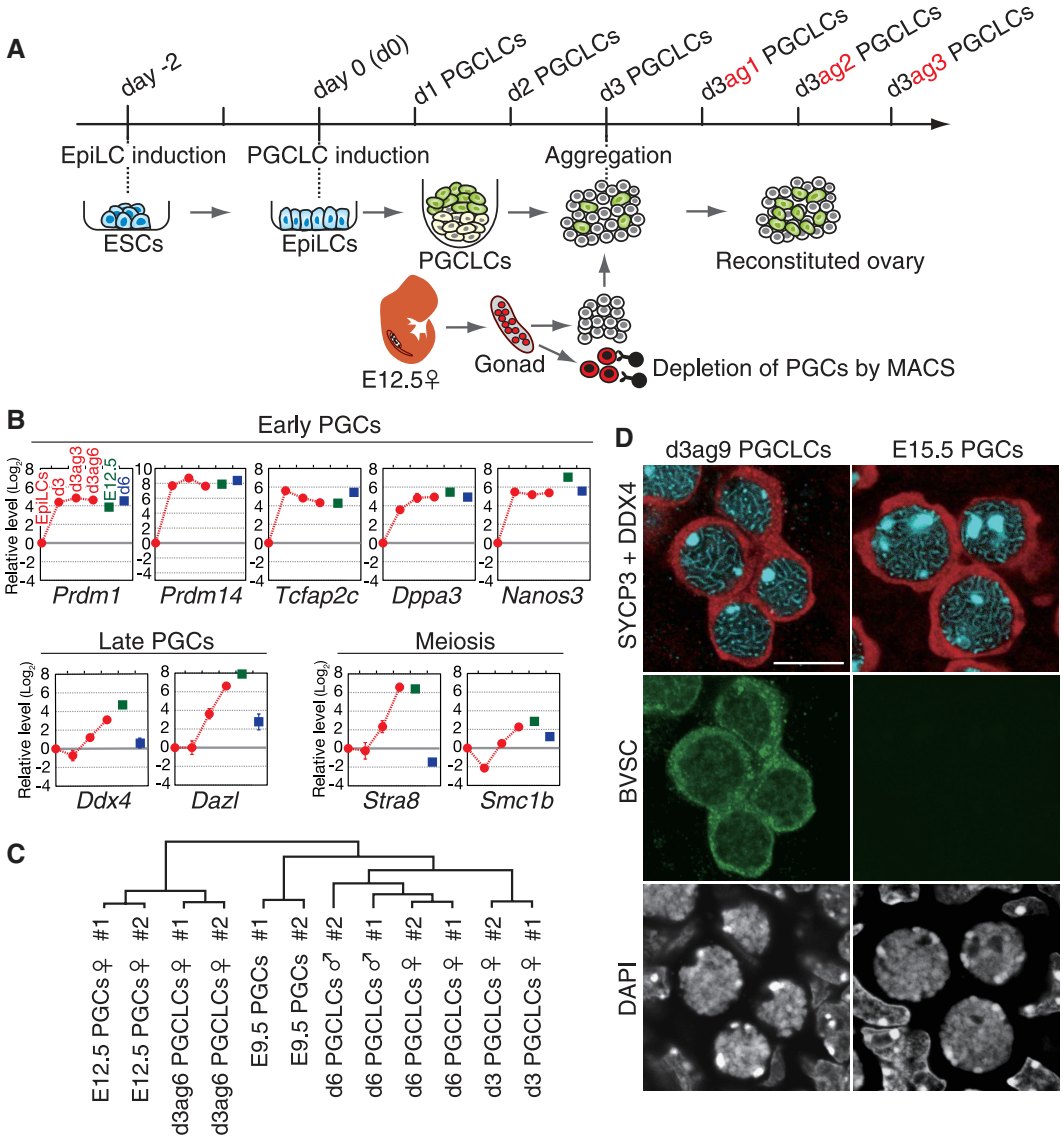

Fig. 1. Female PGCLC development in reconstituted ovaries. (**A**) Scheme for PGCLC induction and ovary reconstitution with d3 PGCLCs. See also fig. S2A. MACS, Magnetic-activated cell sorting. (**B**) Gene expression during PGCLC development and in E12.5 PGCs. For each gene, we calculated the ΔCT (the difference in the threshold cycles) from the average CT values of the two independent housekeeping genes *Arbp* and *Ppia*. The value for EpiLCs was set as 0. As represented in the *Prdm1* panel (upper left), for each point, the average value from two independent experiments is shown on the $\log_2$ scale (with standard deviations) for d3 PGCLC development (EpiLCs, d3, d3ag3, d3ag6 PGCLCs, red circles), E12.5 PGCs (green squares), and d6 PGCLCs (blue squares). (**C**) Hierarchical clustering of microarray data for d3 (female), d6 (male and females), and d3ag6 (female) PGCLCs, as well as E9.5 (mixed) and E12.5 (female) PGCs. (**D**) Expression of DDX4 (DEAD box polypeptide 4, a cytoplasmic RNA helicase expressed in germ cells after ~E11.5) (red), SYCP3 (synaptonemal complex protein 3, a component of the synaptonemal complex between meiotic homologous chromosomes, light blue), and the BVSC (*Blimp1-mVenus* and *stella-ECFP*) reporter (green) and 4′,6-diamidino-2-phenylindole (DAPI) staining (white) of d3ag9 PGCLCs (d3 PGCLCs cultured in the reconstituted ovary for 9 days) and E15.5 PGCs. Scale bar, 10 μm.

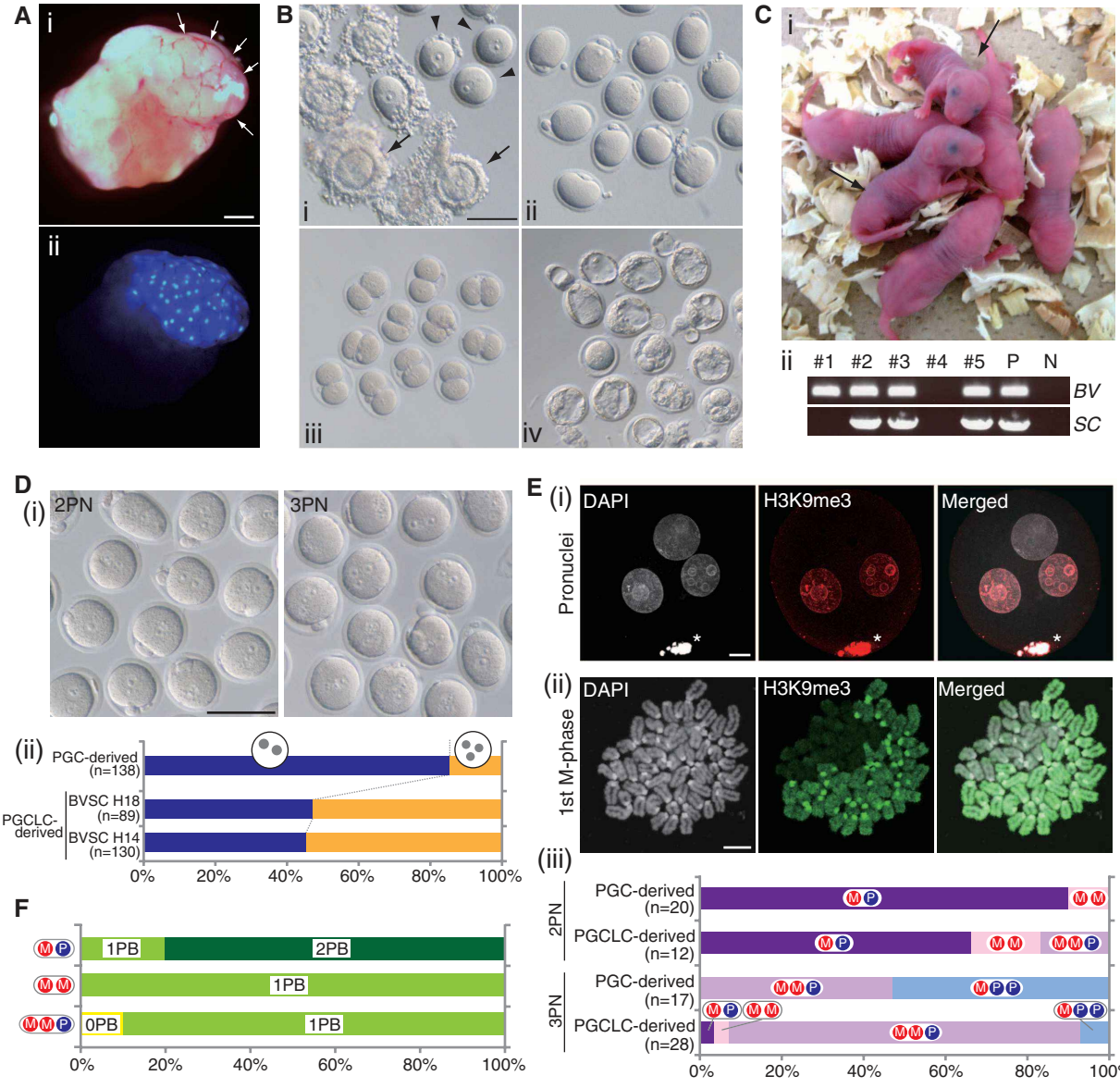

Fig. 2. Oogenesis, embryonic development, and offspring from female PGCLCs. (**A**) Oogenesis by PGCLCs in reconstituted ovaries. (i) Bright-field image of the recipient and reconstituted (arrows) ovary complex. Scale bar, 500 μm. (ii) CFP (cyan fluorescent protein) fluorescence of the complex. (**B**) Maturation by IVM and in vitro development after IVF of PGCLC-derived oocytes. Bright-field images for GV (i) and MII (ii) oocytes, two-cell embryos (iii), and blastocysts (iv). Arrows denote COCs; arrowheads indicate DOs. Scale bar, 100 μm. (**C**) (i) PGCLC-derived offspring (black-eyed, arrow) and (ii) their genotyping by the BVSC transgenes with positive (P) and negative (N) controls. (**D**) (i) PGCLC-derived zygotes and oocytes after IVF bearing 2PN (left) or 3PN (right), judged by visual inspection. Scale bar, 100 μm. (ii) Proportion of 2PN and 3PN zygotes and oocytes after IVF of oocytes from PGCs and PGCLCs (H18 and H14 ESC-derived). n, number of zygotes examined. (**E**) (i) A digynic triploid zygote with one (first) PB (*), stained for H3K9me3 (red) and DAPI (white). (ii) Chromosome spread at the first M phase of a digynic triploid zygote stained for H3K9me3 (green) and DAPI (white). Scale bars in (i) and (ii), 10 μm. (iii) Proportion of the indicated chromosome constitutions in PGCLC- or PGC-derived zygotes and oocytes. M, maternal; P, paternal. (**F**) PBs observed in the PGCLC-derived zygotes. 0PB, no PB detected; 1PB, only the first PB detected; 2PB, the second PB detected.

Table 1. Generation of offspring from oocytes derived from 3-week ovaries, E12.5 PGCs, and PGCLCs. –, not determined; b, black-eyed; al, albino.

Donor	Transplants recovered	Total GVs (/transplant)	MII oocytes (%)	IVF	Fertilized (%)	Culture	Two-cell embryos (%)	Embryos transferred	Pups (%)
Oocytes (3 weeks)	–	165	65 (39.4)	59	57 (96.6)	57	55 (96.5)	55	7 (12.7)
E12.5 PGCs (SG)	15	485 (32.3)	223 (46.0)	223	127 (57.0)	113	85 (75.2)	75	13 (17.3)
d3 PGCLCs (ESCs)	16	535 (33.4)	319 (59.6)	243	204 (84.0)	204	127 (62.3)	127	5 (3.9)
d6 PGCLCs (ESCs)	20	62 (3.1)	28 (45.2)	–	–	–	–	–	–
d4 PGCLCs (iPSCs)	36	1565 (43.5)	507 (32.4)	507	342 (67.5)	236	163 (69.1)	163	14 (b 3; al 11)
E12.5 PGCs*	10	145 (14.5)	67 (46.2)	–	–	–	–	–	–

*PGCs remaining to be sorted out by MACS.

and C, figs. S3 and S4, and supplementary text). We validated that in reconstituted ovaries, d3 and d6 PGCLCs can progress into the zygotene stage of the meiotic prophase [judged by the expression and localization pattern of SYCP3 (synaptonemal complex protein 3) (Fig. 1D, fig. S3, and supplementary text)], demonstrating the meiotic potential of PGCLCs.

To explore the potential of PGCLCs for oogenesis, we generated the reconstituted ovaries with d3 PGCLCs, d6 PGCLCs, and stella-*EGFP* (SG)–positive E12.5 female PGCs (*7*) (5000 PGCLCs or E12.5 PGCs plus 50,000 somatic cells), respectively, and transplanted them at d2 of culture under the ovarian bursa of nude mice (two reconstituted ovaries per recipient ovary). Four weeks and 4 days after transplantation, we isolated the complex of the recipient and reconstituted ovaries. The reconstituted ovaries with PGCLCs, especially those with d3 PGCLCs, exhibited substantial growth, were well vascularized, and exhibited strong SC [*Dppa3*/*stella-ECFP*] fluorescence, which indicates the presence of growing or grown oocytes (Fig. 2A and fig. S5A). Histological sections revealed that the SC-positive donor cells contribute to oocyte-like cells, and nearly all of them reached the fully grown germinal vesicle (GV) stage, bearing multiple layers of granulosa and theca cells similar to the fully grown recipient follicles (fig. S5B). We found no primordial or primary donor-derived follicles (fig. S5, A and B), indicating that PGCLCs underwent oogenesis in a synchronous single wave. Similarly, E12.5 PGCs underwent oogenesis in reconstituted ovaries in a single wave (fig. S5A), which is consistent with a previous observation (*6*).

To evaluate the morphology and efficiency of the formation of GV oocytes by PGCLCs and PGCs, we mechanically isolated follicles and oocytes in the reconstituted ovaries. We also mechanically isolated GV follicles and oocytes in wild-type (WT) ovaries at 3 weeks. The average numbers of d3 PGCLC- and E12.5 PGC-derived GV oocytes per reconstituted ovary were comparable (33.4 and 32.3, respectively), whereas that of d6 PGCLCs was smaller (3.1) (Table 1). This may be partly because d3, but not d6 PGCLCs proliferate robustly in reconstituted ovaries (fig. S2). Whereas most (~65%) of the WT oocytes at 3 weeks were isolated as a cumulus cell-oocyte complex (COC), most (~60%) of the oocytes derived from PGCLCs and PGCs were isolated as denuded oocytes (DOs) (fig. S6A). Moreover, the oocytes derived from the PGCLCs exhibited abnormal elliptical shape at a higher frequency than the oocytes of the other two groups (fig. S6A). These results suggest that, although the development of the PGCLC- and E12.5 PGC-reconstituted ovaries appears grossly normal, it may involve some instability in COC formation and that the GV oocytes from PGCLCs may exhibit some cytoskeletal immaturity and/or fragility with a certain frequency.

We performed in vitro maturation (IVM) and in vitro fertilization (IVF) of the d3 PGCLC- and PGC-derived oocytes and the WT oocytes at 3 weeks (fig. S6B). Despite differences in COC stability and shape, the PGCLC-derived oocytes reached metaphase II (MII), were fertilized, and developed into two-cell embryos with an efficiency comparable to that of oocytes from other sources (Fig. 2B, fig. S6C, and Table 1). Some of the two-cell embryos from the PGCLCs developed further into blastocysts in vitro [19 of 46 (19/46), ~39%] (Fig. 2B). We transferred the two-cell embryos from PGCLCs, as well as those from the other sources, to separate foster mothers. We obtained newborn pups from the two-cell embryos derived from PGCLCs (5/127, ~3.9%), as well as from those derived from E12.5 PGCs (13/75, ~17.3%) and WT 3-week oocytes (7/55, ~12.7%) (Fig. 2C, fig. S7A, and Table 1). All of these offspring grew similarly into adulthood (fig. S7C). The PGCLC-derived offspring bore the BVSC transgenes, a normal imprinting pattern, and full fertility (Fig. 2C and fig. S7, B and D). These findings demonstrate that female PGCLCs induced from ESCs in vitro can form fully functional oocytes.

Nonetheless, it was less efficient to obtain PGCLC-derived pups (~3.9%) than E12.5 PGC- or WT 3-week oocyte-derived pups (~12.7 and ~17.3%, respectively) (Table 1). To gain insight into the underlying mechanisms, we examined the meiosis of the oocytes from PGCLCs. Most PGCLC-derived MII-oocytes induced by IVM bore apparently normal meiotic spindles and the first polar bodies (PBs) (fig. S8A), indicating relatively normal first meiotic division of the PGCLC-derived oocytes. However, when we scrutinized the PGCLC-derived zygotes formed by IVF at the pronuclear stage, we found that about half (~52.8%) of them had three pronuclei (3PN), whereas a majority (~85.5%) of PGC-derived oocytes had a normal two-pronuclear

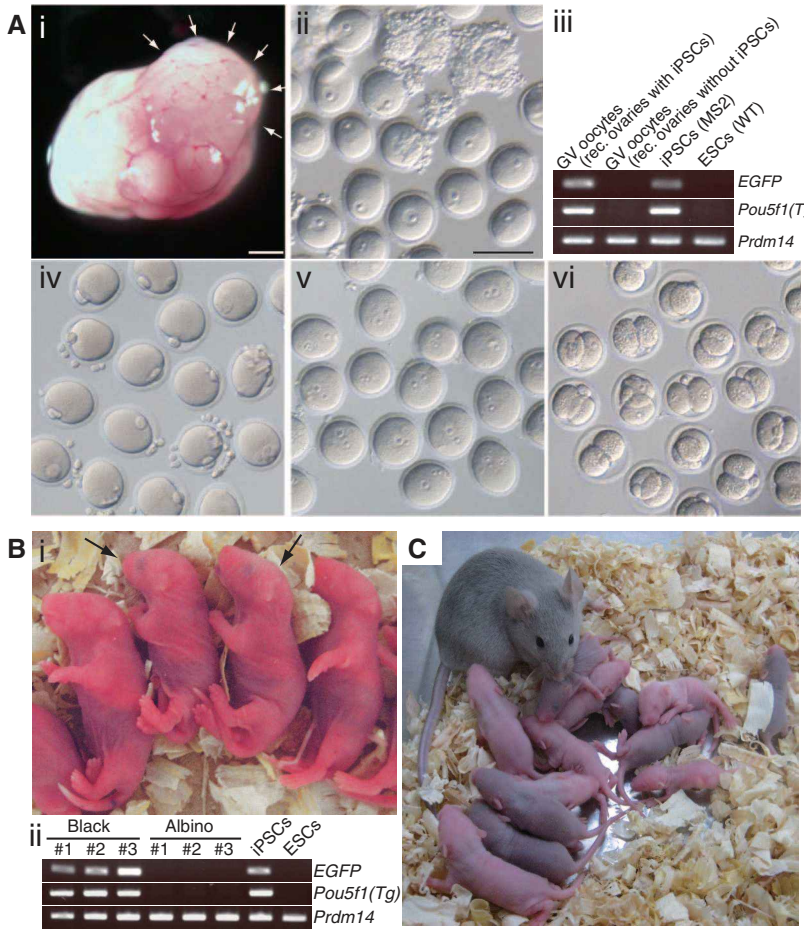

Fig. 3. Oogenesis, embryonic development, and offspring from female iPSC-derived PGCLCs. (**A**) Oogenesis and embryonic development from iPSC-derived PGCLCs. (i) Bright-field image of the recipient and reconstituted (arrows) ovary complex. Scale bar, 500 μm. (ii) GV oocytes isolated from reconstituted ovaries. Scale bar, 100 μm. (iii) Genotyping by indicated elements of GV oocytes from reconstituted ovaries with iPSC-derived PGCLCs or from control ovaries, iPSCs, and WT ESCs. (iv to vi) MII oocytes (iv), zygotes (v), and two-cell embryos (vi) from the GV oocytes in (ii). (**B**) (i) Black-eyed offspring from iPSC-derived PGCLCs (arrows) and (ii) their genotyping by indicated elements, with genotyping of albino offspring, iPSCs, and WT ESCs. (**C**) Fertile female offspring from iPSC-derived PGCLCs.

(2PN) phenotype (Fig. 2D). The H14 ESC-derived PGCLC-derived zygotes showed a similar phenotype (Fig. 2D), indicating that the emergence of zygotes and oocytes bearing 3PN after IVF at a higher ratio is a feature of oocytes derived from female ESCs. Most PGCLC-derived 3PN zygotes had two maternal (M) chromosomes positive for histone H3 lysine nine trimethylation (H3K9me3) (*8*) and one paternal (P) chromosome, whereas about ~65% of the 2PN zygotes from PGCLCs had one M and one P chromosome and the rest had either two Ms or two Ms and one P (Fig. 2E). All of the 3PN zygotes examined (10/10) failed to extrude the second PBs and carried the triploid chromosomes into two-cell embryos (Fig. 2F and fig. S8, B and C). These findings indicate that a subset of the zygotes and oocytes derived from PGCLCs are unable to extrude the second PBs, resulting, after IVF, in the digynic triploid (MMP) phenotype or the digynic diploid (MM) phenotype with a failure in fertilization. This defect contributes to a low birth rate from the two-cell embryos derived from PGCLCs (Table 1). Consistent with these findings and the fact that the triploidy is incompatible with mouse development (*9*), all of the offspring from PGCLC-derived oocytes exhibited a normal diploid karyotype (fig. S8D).

We examined whether female iPSCs could similarly be induced into fully functional oocytes. We induced the MS2 iPSCs (derived from female mouse embryonic fibroblasts, mixed background with C57BL/6, and bearing *Pou5f1-EGFP* transgenes) (*10*) into PGCLCs. We purified integrin-β3– and SSEA1-positive cells, which are nearly identical to cells with BV positivity (*1*), from the floating aggregates containing d4 PGCLCs (we used d4 PGCLCs because integrin-β3 exhibits specific expression after d4 of PGCLC induction) (fig. S9, A and B) and generated reconstituted ovaries. As a control, we generated reconstituted ovaries without the iPSC-derived PGCLCs, but with a small number of unsorted endogenous PGCs (ICR background). After transplantation, the reconstituted ovaries with the iPSC-derived PGCLCs bore many more growing or grown follicles (43.5 per transplant) than the controls (14.5 per transplant) (Fig. 3A and Table 1), suggesting that the iPSC-derived PGCLCs contributed successfully to oogenesis. Although the *Pou5f1-EGFP* transgenes did not show detectable fluorescence in the reconstituted ovaries (fig. S9, C to F), the GV oocytes from reconstituted ovaries containing the iPSC-derived PGCLCs specifically bore the *EGFP* and *Pou5f1* retrovirus transgenes, as did the original MS2 iPSCs (Fig. 3A), demonstrating the contribution of the iPSC-derived PGCLCs to oogenesis. We performed IVM and IVF using these oocytes and transferred two-cell embryos derived from zygotes with 2PN to foster mothers (Fig. 3A). We obtained three offspring with black eyes, which bore the *EGFP* and the *Pou5f1* transgenes and grew into fertile adults (Fig. 3, B and C, and fig. S9G). We conclude that like female ESCs, female iPSCs can be induced into PGCLCs in vitro, which, in turn, can mature into properly functioning oocytes.

A previous study showed that ESCs could differentiate into oocyte-like cells in culture, although these cells did not contribute to offspring (*11*). We demonstrate here that female ESCs and iPSCs were induced into PGCLCs, which underwent proper development in reconstituted ovaries in vitro and matured further into fully functional GV oocytes upon transplantation in vivo. Combined with our previous study (*1*), reconstitution of the essential first step of pluripotent stem cell–based gamete production in vitro has been established in both sexes. Unlike the E12.5 PGC-derived oocytes and zygotes, about half of the PGCLC-derived oocytes and zygotes failed to extrude the second PBs. The underlying mechanism of this failure requires further investigation. Combined with previous studies (*12*, *13*), our system serves as a robust foundation to investigate and further reconstitute female germline development in vitro, not only in mice, but also in other mammals, including humans.

References and Notes

1. K. Hayashi, H. Ohta, K. Kurimoto, S. Aramaki, M. Saitou, *Cell* **146**, 519 (2011).
2. I. Zvetkova *et al.*, *Nat. Genet.* **37**, 1274 (2005).
3. H. Sasaki, Y. Matsui, *Nat. Rev. Genet.* **9**, 129 (2008).
4. Y. Ohinata, M. Sano, M. Shigeta, K. Yamanaka, M. Saitou, *Reproduction* **136**, 503 (2008).
5. K. Hashimoto, M. Noguchi, N. Nakatsuji, *Dev. Growth Differ.* **34**, 233 (1992).
6. S. Matoba, A. Ogura, *Biol. Reprod.* **84**, 631 (2011).
7. B. Payer *et al.*, *Genesis* **44**, 75 (2006).
8. F. Santos, A. H. Peters, A. P. Otte, W. Reik, W. Dean, *Dev. Biol.* **280**, 225 (2005).
9. M. H. Kaufman, S. Speirs, *Development* **101**, 383 (1987).
10. J. Silva *et al.*, *Cell* **138**, 722 (2009).
11. K. Hübner *et al.*, *Science* **300**, 1251 (2003).
12. J. J. Eppig, M. J. O'Brien, *Biol. Reprod.* **54**, 197 (1996).
13. Y. Obata, T. Kono, I. Hatada, *Nature* **418**, 497 (2002).

Acknowledgments: We thank J. Silva and A. Smith for the MS2 female iPSCs, K. Okita and S. Yamanaka for the female iPSCs, and Y. Matsui for the GOF18-ESCs. We also thank S. Matoba and A. Ogura for their advice on ovary reconstitution, S. Aramaki and Y. Ishikura for assistance, and T. Mori for encouragement. This study was supported in part by a Grant-in-Aid from the Ministry of Education, Culture, Sports, Science, and Technology of Japan; by JST-PRESTO/CREST/ERATO; by the Takeda Science Foundation; and by the the Academia for Repro-regenerative Medicine. The accession number for the microarray data presented in this study is GSE40716 [Gene Expression Omnibus (GEO) database].

Supplementary Materials

www.sciencemag.org/cgi/content/full/science.1226889/DC1
Materials and Methods
Supplementary Text
Figs. S1 to S9
Table S1
References (*14*–*36*)

3 July 2012; accepted 18 September 2012
Published online 4 October 2012;
10.1126/science.1226889

A Genomic Regulatory Element That Directs Assembly and Function of Immune-Specific AP-1–IRF Complexes

Elke Glasmacher,[1]* Smita Agrawal,[1]* Abraham B. Chang,[1]* Theresa L. Murphy,[2]* Wenwen Zeng,[1]* Bryan Vander Lugt,[1] Aly A. Khan,[3] Maria Ciofani,[4] Chauncey J. Spooner,[1] Sascha Rutz,[1] Jason Hackney,[5] Roza Nurieva,[6] Carlos R. Escalante,[7] Wenjun Ouyang,[1] Dan R. Littman,[4] Kenneth M. Murphy,[2]† Harinder Singh[1]†

Interferon regulatory factor 4 (IRF4) and IRF8 regulate B, T, macrophage, and dendritic cell differentiation. They are recruited to cis-regulatory Ets-IRF composite elements by PU.1 or Spi-B. How these IRFs target genes in most T cells is enigmatic given the absence of specific Ets partners. Chromatin immunoprecipitation sequencing in T helper 17 (T_H17) cells reveals that IRF4 targets sequences enriched for activating protein 1 (AP-1)–IRF composite elements (AICEs) that are co-bound by BATF, an AP-1 factor required for T_H17, B, and dendritic cell differentiation. IRF4 and BATF bind cooperatively to structurally divergent AICEs to promote gene activation and T_H17 differentiation. The AICE motif directs assembly of IRF4 or IRF8 with BATF heterodimers and is also used in T_H2, B, and dendritic cells. This genomic regulatory element and cognate factors appear to have evolved to integrate diverse immunomodulatory signals.

Interferon regulatory factor 4 (IRF4) and IRF8 are evolutionarily diverged members of the IRF family of transcription factors (*1*). Unlike other members, which are ubiquitously expressed, IRF4 and IRF8 are largely restricted to the immune system and play key roles in the differentiation and functioning of innate and adaptive immune cells (*2*, *3*). IRF4 is required for B cells to undergo class switch recombination and plasma cell differentiation (*4*, *5*). It